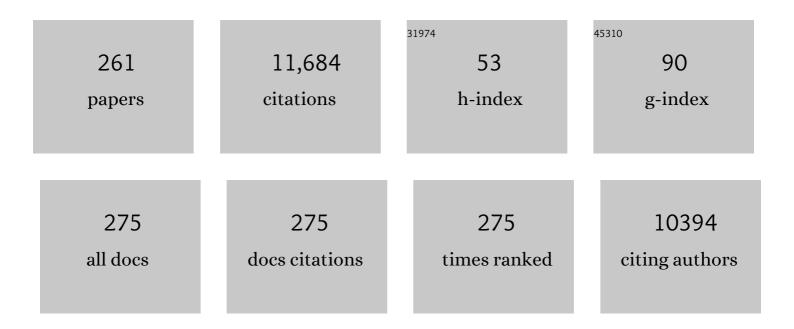
List of Publications by Year in descending order

Source: https://exaly.com/author-pdf/6035507/publications.pdf Version: 2024-02-01



#	Article	IF	CITATIONS
1	Development of a 4-D digital mouse phantom for molecular imaging research. Molecular Imaging and Biology, 2004, 6, 149-159.	2.6	363
2	MRI of the lungs using hyperpolarized noble gases. Magnetic Resonance in Medicine, 2002, 47, 1029-1051.	3.0	362
3	Waxholm Space atlas of the Sprague Dawley rat brain. NeuroImage, 2014, 97, 374-386.	4.2	321
4	Rapid calculation of T1 using variable flip angle gradient refocused imaging. Magnetic Resonance Imaging, 1987, 5, 201-208.	1.8	318
5	Morphologic Phenotyping with MR Microscopy: The Visible Mouse. Radiology, 2002, 222, 789-793.	7.3	244
6	Waxholm Space: An image-based reference for coordinating mouse brain research. NeuroImage, 2010, 53, 365-372.	4.2	236
7	A Liposomal Nanoscale Contrast Agent for Preclinical CT in Mice. American Journal of Roentgenology, 2006, 186, 300-307.	2.2	226
8	Pattern formation in flowing sand. Physical Review Letters, 1989, 62, 2825-2828.	7.8	215
9	Imaging alveolar-capillary gas transfer using hyperpolarized 129Xe MRI. Proceedings of the National Academy of Sciences of the United States of America, 2006, 103, 18278-18283.	7.1	210
10	High-field (9.4T) MRI of brain dysmyelination by quantitative mapping of magnetic susceptibility. NeuroImage, 2011, 56, 930-938.	4.2	199
11	A Diffusion MRI Tractography Connectome of the Mouse Brain and Comparison with Neuronal Tracer Data. Cerebral Cortex, 2015, 25, 4628-4637.	2.9	193
12	Spatially resolved measurements of hyperpolarized gas properties in the lung in vivo. Part I: Diffusion coefficient. Magnetic Resonance in Medicine, 1999, 42, 721-728.	3.0	170
13	A diffusion tensor MRI atlas of the postmortem rhesus macaque brain. NeuroImage, 2015, 117, 408-416.	4.2	169
14	Intracardiac septation requires hedgehog-dependent cellular contributions from outside the heart. Development (Cambridge), 2008, 135, 1887-1895.	2.5	161
15	Sparseness prior based iterative image reconstruction for retrospectively gated cardiac micro T. Medical Physics, 2007, 34, 4476-4483.	3.0	152
16	4-D Micro-CT of the Mouse Heart. Molecular Imaging, 2005, 4, 153535002005041.	1.4	139
17	Magnetic Resonance Microscopy Defines Ethanolâ€Induced Brain Abnormalities in Prenatal Mice: Effects of Acute Insult on Gestational Day 8. Alcoholism: Clinical and Experimental Research, 2009, 33, 1001-1011.	2.4	127
18	Ethanol-Induced Face-Brain Dysmorphology Patterns Are Correlative and Exposure-Stage Dependent. PLoS ONE, 2012, 7, e43067.	2.5	122

#	Article	IF	CITATIONS
19	High-throughput morphologic phenotyping of the mouse brain with magnetic resonance histology. NeuroImage, 2007, 37, 82-89.	4.2	115
20	Magnetic Resonance Microscopy Defines Ethanolâ€Induced Brain Abnormalities in Prenatal Mice: Effects of Acute Insult on Gestational Day 7. Alcoholism: Clinical and Experimental Research, 2010, 34, 98-111.	2.4	113
21	Magnetic resonance histology for morphologic phenotyping. Journal of Magnetic Resonance Imaging, 2002, 16, 423-429.	3.4	112
22	Digital Atlasing and Standardization in the Mouse Brain. PLoS Computational Biology, 2011, 7, e1001065.	3.2	109
23	High-resolution magnetic resonance histology of the embryonic and neonatal mouse: A 4D atlas and morphologic database. Proceedings of the National Academy of Sciences of the United States of America, 2008, 105, 12331-12336.	7.1	108
24	A quantitative magnetic resonance histology atlas of postnatal rat brain development with regional estimates of growth and variability. NeuroImage, 2013, 71, 196-206.	4.2	102
25	MR microscopy of lung airways with hyperpolarized3He. Magnetic Resonance in Medicine, 1998, 39, 79-84.	3.0	95
26	Methodology for the measurement and analysis of relaxation times in proton imaging. Magnetic Resonance Imaging, 1987, 5, 209-220.	1.8	94
27	A multidimensional magnetic resonance histology atlas of the Wistar rat brain. NeuroImage, 2012, 62, 1848-1856.	4.2	91
28	Magnetic Resonance Microscopy of the C57BL Mouse Brain. NeuroImage, 2000, 11, 601-611.	4.2	90
29	Automated segmentation of neuroanatomical structures in multispectral MR microscopy of the mouse brain. Neurolmage, 2005, 27, 425-435.	4.2	86
30	Abnormal water metabolism in mice lacking the type 1A receptor for ANG II. American Journal of Physiology - Renal Physiology, 2000, 278, F75-F82.	2.7	84
31	Evaluation of Tumor Microenvironment in an Animal Model using a Nanoparticle Contrast Agent in Computed Tomography Imaging. Academic Radiology, 2011, 18, 20-30.	2.5	84
32	Postmortem diffusion MRI of the human brainstem and thalamus for deep brain stimulator electrode localization. Human Brain Mapping, 2015, 36, 3167-3178.	3.6	84
33	3D fiber tractography with susceptibility tensor imaging. NeuroImage, 2012, 59, 1290-1298.	4.2	82
34	Spatially resolved measurements of hyperpolarized gas properties in the lung in vivo. Part II:T?2. Magnetic Resonance in Medicine, 1999, 42, 729-737.	3.0	81
35	MR-compatible ventilator for small animals: computer-controlled ventilation for proton and noble gas imaging. Magnetic Resonance Imaging, 2000, 18, 753-759.	1.8	75
36	Optimization of Eight-Element Multi–Detector Row Helical CT Technology for Evaluation of the Abdomen. Radiology, 2003, 227, 739-745.	7.3	73

#	Article	IF	CITATIONS
37	Magnetic resonance microscopy of embryos. Computerized Medical Imaging and Graphics, 1996, 20, 483-490.	5.8	72

Diabetes Insipidus in Uricase-Deficient Mice: A Model for Evaluating Therapy with Poly(Ethylene) Tj ETQq0 0 0 rgBT (Overlock 10 Tf 50 70

39	Superparamagnetic Iron Oxide Labeling and Transplantation of Adipose-Derived Stem Cells in Middle Cerebral Artery Occlusion-Injured Mice. American Journal of Roentgenology, 2007, 188, 1101-1108.	2.2	68
40	Signal Dynamics in Magnetic Resonance Imaging of the Lung with Hyperpolarized Noble Gases. Journal of Magnetic Resonance, 1998, 135, 133-143.	2.1	65
41	The use of gradient flow compensation to separate diffusion and microcirculatory flow in MRI. Magnetic Resonance in Medicine, 1991, 17, 95-107.	3.0	63
42	Dynamics of magnetization in hyperpolarized gas MRI of the lung. Magnetic Resonance in Medicine, 1997, 38, 66-71.	3.0	63
43	Functional MR microscopy of the lung using hyperpolarized3He. Magnetic Resonance in Medicine, 1999, 41, 787-792.	3.0	62
44	Purkinje cell loss in experimental autoimmune encephalomyelitis. NeuroImage, 2009, 48, 637-651.	4.2	62
45	Microscopic diffusion tensor imaging of the mouse brain. NeuroImage, 2010, 50, 465-471.	4.2	62
46	Automated segmentation of the actively stained mouse brain using multi-spectral MR microscopy. NeuroImage, 2008, 39, 136-145.	4.2	61
47	4-D micro-CT of the mouse heart. Molecular Imaging, 2005, 4, 110-6.	1.4	61
48	Fiber-optic stethoscope: A cardiac monitoring and gating system for magnetic resonance microscopy. Magnetic Resonance in Medicine, 2002, 47, 314-321.	3.0	60
49	Neuroanatomical phenotypes in the Reeler mouse. NeuroImage, 2007, 34, 1363-1374.	4.2	60
50	Computed Tomography Imaging of Primary Lung Cancer in Mice Using a Liposomal-Iodinated Contrast Agent. PLoS ONE, 2012, 7, e34496.	2.5	60
51	Whole mouse brain structural connectomics using magnetic resonance histology. Brain Structure and Function, 2018, 223, 4323-4335.	2.3	60
52	High-resolution imaging of murine myocardial infarction with delayed-enhancement cine micro-CT. American Journal of Physiology - Heart and Circulatory Physiology, 2007, 292, H3172-H3178.	3.2	59
53	Dual-Energy Computed Tomography Imaging of Atherosclerotic Plaques in a Mouse Model Using a Liposomal-Iodine Nanoparticle Contrast Agent. Circulation: Cardiovascular Imaging, 2013, 6, 285-294.	2.6	59
	³ He MRI in mouse models of asthma. Magnetic Resonance in Medicine, 2007, 58, 893-900.	3.0	57

#	Article	IF	CITATIONS
55	Dual-Energy Micro-Computed Tomography Imaging of Radiation-Induced Vascular Changes in Primary Mouse Sarcomas. International Journal of Radiation Oncology Biology Physics, 2013, 85, 1353-1359.	0.8	57
56	Magnetic resonance microscopyâ€based analyses of the brains of normal and ethanolâ€exposed fetal mice. Birth Defects Research Part A: Clinical and Molecular Teratology, 2010, 88, 953-964.	1.6	56
57	Mapping the human subcortical auditory system using histology, postmortem MRI and in vivo MRI at 7T. ELife, 2019, 8, .	6.0	56
58	Mechanical Ventilation for Imaging the Small Animal Lung. ILAR Journal, 2002, 43, 159-174.	1.8	55
59	Magnetic resonance angiography with hyperpolarized129Xe dissolved in a lipid emulsion. Magnetic Resonance in Medicine, 1999, 41, 1058-1064.	3.0	54
60	Registered1H and3He magnetic resonance microscopy of the lung. Magnetic Resonance in Medicine, 2001, 45, 365-370.	3.0	54
61	Geometric calibration for a dual tube/detector micro T system. Medical Physics, 2008, 35, 1820-1829.	3.0	53
62	Three-dimensional MRI microscopy of the normal rat brain. Magnetic Resonance in Medicine, 1987, 4, 351-365.	3.0	52
63	Measurement of regional lung function in rats using hyperpolarized3helium dynamic MRI. Magnetic Resonance in Medicine, 2003, 49, 78-88.	3.0	52
64	A dual micro-CT system for small animal imaging. Proceedings of SPIE, 2008, 6913, 691342.	0.8	51
65	Diffusion Tensor Imaging Reveals White Matter Injury in a Rat Model of Repetitive Blast-Induced Traumatic Brain Injury. Journal of Neurotrauma, 2014, 31, 938-950.	3.4	51
66	Neurite orientation dispersion and density imaging of mouse brain microstructure. Brain Structure and Function, 2019, 224, 1797-1813.	2.3	51
67	Magnetic resonance imaging in multiple sclerosis: Decreased signal in thalamus and putamen. Annals of Neurology, 1987, 22, 546-550.	5.3	50
68	Measurements of hyperpolarized gas properties in the lung. part III:3HeT1. Magnetic Resonance in Medicine, 2001, 45, 421-430.	3.0	50
69	Susceptibility tensor imaging of the kidney and its microstructural underpinnings. Magnetic Resonance in Medicine, 2015, 73, 1270-1281.	3.0	50
70	Diffusionâ€weighted MR microscopy with fast spinâ€echo. Magnetic Resonance in Medicine, 1993, 30, 201-206.	3.0	49
71	Reduction of ringing and blurring artifacts in fast spin-echo imaging. Journal of Magnetic Resonance Imaging, 1993, 3, 803-807.	3.4	49
72	Effects of breathing and cardiac motion on spatial resolution in the microscopic imaging of rodents. Magnetic Resonance in Medicine, 2005, 53, 858-865.	3.0	49

#	Article	IF	CITATIONS
73	Magnetic resonance imaging at microscopic resolution reveals subtle morphological changes in a mouse model of dopaminergic hyperfunction. NeuroImage, 2005, 26, 83-90.	4.2	49
74	Quantitative magnetic susceptibility of the developing mouse brain reveals microstructural changes in the white matter. NeuroImage, 2014, 88, 134-142.	4.2	49
75	Tumor location, but not H3.3K27M, significantly influences the blood–brain-barrier permeability in a genetic mouse model of pediatric high-grade glioma. Journal of Neuro-Oncology, 2016, 126, 243-251.	2.9	49
76	Genetic dissection of the mouse brain using high-field magnetic resonance microscopy. Neurolmage, 2009, 45, 1067-1079.	4.2	48
77	Microscopic diffusion tensor atlas of the mouse brain. NeuroImage, 2011, 56, 1235-1243.	4.2	48
78	Tumor imaging in small animals with a combined micro-CT/micro-DSA system using iodinated conventional and blood pool contrast agents. Contrast Media and Molecular Imaging, 2006, 1, 153-164.	0.8	47
79	Adult rat cortical thickness changes across age and following adolescent intermittent ethanol treatment. Addiction Biology, 2017, 22, 712-723.	2.6	47
80	Performance of a high-temperature superconducting probe for in vivo microscopy at 2.0 T. Magnetic Resonance in Medicine, 1999, 41, 72-79.	3.0	46
81	Least-Square NUFFT Methods Applied to 2-D and 3-D Radially Encoded MR Image Reconstruction. IEEE Transactions on Biomedical Engineering, 2009, 56, 1134-1142.	4.2	46
82	Contrastâ€enhanced in vivo magnetic resonance microscopy of the mouse brain enabled by noninvasive opening of the bloodâ€brain barrier with ultrasound. Magnetic Resonance in Medicine, 2010, 64, 995-1004.	3.0	46
83	Magnetic resonance imaging of embryos: an Internet resource for the study of embryonic development. Computerized Medical Imaging and Graphics, 1999, 23, 33-40.	5.8	45
84	Myocardial volume and organization are changed by failure of addition of secondary heart field myocardium to the cardiac outflow tract. Developmental Dynamics, 2003, 228, 152-160.	1.8	45
85	Optimization of Multiplanar Reformations from Isotropic Data Sets Acquired with 16–Detector Row Helical CT Scanner. Radiology, 2006, 238, 292-299.	7.3	45
86	Magnetic resonance microscopy-based analyses of the neuroanatomical effects of gestational day 9 ethanol exposure in mice. Neurotoxicology and Teratology, 2013, 39, 77-83.	2.4	45
87	Quantitative susceptibility mapping of kidney inflammation and fibrosis in type 1 angiotensin receptorâ€deficient mice. NMR in Biomedicine, 2013, 26, 1853-1863.	2.8	45
88	MR microimaging of the lung using volume projection encoding. Magnetic Resonance in Medicine, 1997, 38, 938-942.	3.0	44
89	Fourâ€dimensional MR microscopy of the mouse heart using radial acquisition and liposomal gadolinium contrast agent. Magnetic Resonance in Medicine, 2008, 60, 111-118.	3.0	44
90	Magnetic resonance imaging of leaves. New Phytologist, 1993, 123, 769-774.	7.3	43

#	Article	IF	CITATIONS
91	Staining methods for magnetic resonance microscopy of the rat fetus. Journal of Magnetic Resonance Imaging, 2007, 25, 1192-1198.	3.4	43
92	Assessing Cardiac Injury in Mice With Dual Energy-MicroCT, 4D-MicroCT, and MicroSPECT Imaging After Partial Heart Irradiation. International Journal of Radiation Oncology Biology Physics, 2014, 88, 686-693.	0.8	43
93	Imaging whole-brain cytoarchitecture of mouse with MRI-based quantitative susceptibility mapping. NeuroImage, 2016, 137, 107-115.	4.2	43
94	Remote sites of structural atrophy predict later amyloid formation in a mouse model of Alzheimer's disease. Neurolmage, 2010, 50, 416-427.	4.2	42
95	Small Animal Multivariate Brain Analysis (SAMBA) – a High Throughput Pipeline with a Validation Framework. Neuroinformatics, 2019, 17, 451-472.	2.8	42
96	Applications of Magnetic Resonance Microscopy. Toxicologic Pathology, 2004, 32, 42-48.	1.8	41
97	Sensitivity and resolution in 3D NMR microscopy of the lung with hyperpolarized noble gases. Magnetic Resonance in Medicine, 1999, 41, 800-808.	3.0	39
98	EnhancedT2 contrast for MR histology of the mouse brain. Magnetic Resonance in Medicine, 2006, 56, 717-725.	3.0	38
99	Imaging Methods for Morphological and Functional Phenotyping of the Rodent Heart. Toxicologic Pathology, 2006, 34, 111-117.	1.8	38
100	Optical clearing of unsectioned specimens for three-dimensional imaging via optical transmission and emission tomography. Journal of Biomedical Optics, 2008, 13, 021113.	2.6	38
101	In Situ Magnetic Resonance Microscopy. Investigative Radiology, 1987, 22, 965-968.	6.2	37
102	DISTINGUISHING PLANT TISSUES WITH MAGNETIC RESONANCE MICROSCOPY. American Journal of Botany, 1991, 78, 1704-1711.	1.7	37
103	High-Field MR microscopy using fast spin-echoes. Magnetic Resonance in Medicine, 1993, 30, 60-67.	3.0	37
104	MR Microscopy of the Rat Carotid Artery after Balloon Injury by Using an Implanted Imaging Coil. Magnetic Resonance in Medicine, 1995, 33, 785-789.	3.0	37
105	Improved preparation of chick embryonic samples for magnetic resonance microscopy. Magnetic Resonance in Medicine, 2003, 49, 1192-1195.	3.0	37
106	Ventilation-synchronous magnetic resonance microscopy of pulmonary structure and ventilation in mice. Magnetic Resonance in Medicine, 2005, 53, 69-75.	3.0	37
107	4D micro-CT for cardiac and perfusion applications with view under sampling. Physics in Medicine and Biology, 2011, 56, 3351-3369.	3.0	37
108	Three-dimensional reconstruction in free-space whole-body fluorescence tomography of mice using optically reconstructed surface and atlas anatomy. Journal of Biomedical Optics, 2009, 14, 064010.	2.6	36

#	Article	IF	CITATIONS
109	Highâ€resolution magnetic resonance angiography in the mouse using a nanoparticle bloodâ€pool contrast agent. Magnetic Resonance in Medicine, 2009, 62, 1447-1456.	3.0	36
110	Investigating the tradeoffs between spatial resolution and diffusion sampling for brain mapping with diffusion tractography: Time well spent?. Human Brain Mapping, 2014, 35, 5667-5685.	3.6	36
111	Neurotoxicity of carbonyl sulfide in F344 rats following inhalation exposure for up to 12 weeks. Toxicology and Applied Pharmacology, 2004, 200, 131-145.	2.8	35
112	MR microscopy of chick embryo vasculature. Journal of Magnetic Resonance Imaging, 1992, 2, 237-240.	3.4	34
113	Susceptibility tensor imaging and tractography of collagen fibrils in the articular cartilage. Magnetic Resonance in Medicine, 2017, 78, 1683-1690.	3.0	34
114	Magnetic Resonance Microscopy of the Rat Thorax and Abdomen. Investigative Radiology, 1986, 21, 843-846.	6.2	33
115	Population-averaged diffusion tensor imaging atlas of the Sprague Dawley rat brain. NeuroImage, 2011, 58, 975-983.	4.2	33
116	Magnetic Resonance Histology of Age-Related Nephropathy in the Sprague Dawley Rat. Toxicologic Pathology, 2012, 40, 764-778.	1.8	33
117	Anatomical and functional imaging of myocardial infarction in mice using micro T and eXIA 160 contrast agent. Contrast Media and Molecular Imaging, 2014, 9, 161-168.	0.8	33
118	Variability and heritability of mouse brain structure: Microscopic MRI atlases and connectomes for diverse strains. NeuroImage, 2020, 222, 117274.	4.2	33
119	Magnetic Resonance Microscopy in Basic Studies of Brain Structure and Function ^{<i>a</i>,^{<i>b</i>}. Annals of the New York Academy of Sciences, 1997, 820, 139-148.}	3.8	32
120	Time-course imaging of rat embryos in utero with magnetic resonance microscopy. Magnetic Resonance in Medicine, 1998, 39, 673-677.	3.0	32
121	Mixing oxygen with hyperpolarized3He for small-animal lung studies. NMR in Biomedicine, 2000, 13, 202-206.	2.8	32
122	Improving temporal resolution of pulmonary perfusion imaging in rats using the partially separable functions model. Magnetic Resonance in Medicine, 2010, 64, 1162-1170.	3.0	32
123	Prenatal alcohol exposure reduces magnetic susceptibility contrast and anisotropy in the white matter of mouse brains. NeuroImage, 2014, 102, 748-755.	4.2	32
124	Quantitative mouse brain phenotyping based on single and multispectral MR protocols. NeuroImage, 2012, 63, 1633-1645.	4.2	31
125	T1ϕrelaxation and its application to MR histology. Magnetic Resonance in Medicine, 1996, 35, 781-786.	3.0	30
126	3-Dimensional visualization of lesions in rat brain using magnetic resonance imaging microscopy. NeuroReport, 1999, 10, 737-741.	1.2	29

#	Article	IF	CITATIONS
127	A MICRO–COMPUTED TOMOGRAPHY–BASED METHOD FOR THE MEASUREMENT OF PULMONARY COMPLIANCE IN HEALTHY AND BLEOMYCIN–EXPOSED MICE. Experimental Lung Research, 2007, 33, 169-183.	1.2	29
128	Lung perfusion imaging in small animals using 4D micro T at heartbeat temporal resolution. Medical Physics, 2010, 37, 54-62.	3.0	29
129	Cytoarchitecture of the mouse brain by high resolution diffusion magnetic resonance imaging. NeuroImage, 2020, 216, 116876.	4.2	29
130	Magnetic Resonance Microscopy-A New Tool for the Toxicologic Pathologist. Toxicologic Pathology, 1996, 24, 36-44.	1.8	28
131	Imaging inflammation: Direct visualization of perivascular cuffing in EAE by magnetic resonance microscopy. Journal of Magnetic Resonance Imaging, 2002, 16, 28-36.	3.4	28
132	Cine magnetic resonance microscopy of the rat heart using cardiorespiratory-synchronous projection reconstruction. Journal of Magnetic Resonance Imaging, 2004, 20, 31-38.	3.4	28
133	Dynamic lung morphology of methacholine-induced heterogeneous bronchoconstriction. Magnetic Resonance in Medicine, 2004, 52, 1080-1086.	3.0	28
134	A Probe for Specimen Magnetic Resonance Microscopy. Investigative Radiology, 1992, 27, 157-164.	6.2	27
135	Measurement of fat/water ratios in rat liver using 3D three-point dixon MRI. Magnetic Resonance in Medicine, 2004, 51, 697-702.	3.0	27
136	MRI tools for assessment of microstructure and nephron function of the kidney. American Journal of Physiology - Renal Physiology, 2016, 311, F1109-F1124.	2.7	27
137	Postmortem diffusion MRI of the entire human spinal cord at microscopic resolution. NeuroImage: Clinical, 2018, 18, 963-971.	2.7	27
138	Three dimensional magnetic resonance microangiography of rat neurovasculature. Magnetic Resonance in Medicine, 1994, 32, 199-205.	3.0	26
139	Left ventricle volume measurements in cardiac micro-CT: The impact of radiation dose and contrast agent. Computerized Medical Imaging and Graphics, 2008, 32, 239-250.	5.8	26
140	A High-Precision Contrast Injector for Small Animal X-Ray Digital Subtraction Angiography. IEEE Transactions on Biomedical Engineering, 2008, 55, 1082-1091.	4.2	26
141	Pulmonary perfusion imaging in the rodent lung using dynamic contrastâ€enhanced MRI. Magnetic Resonance in Medicine, 2008, 59, 289-297.	3.0	25
142	Dual-energy micro-CT imaging for differentiation of iodine- and gold-based nanoparticles. Proceedings of SPIE, 2011, , .	0.8	25
143	4D micro-CT using fast prospective gating. Physics in Medicine and Biology, 2012, 57, 257-271.	3.0	25
144	Three-dimensional imaging of xenograft tumors using optical computed and emission tomography. Medical Physics, 2006, 33, 3193-3202.	3.0	24

9

#	Article	IF	CITATIONS
145	Design of a superconducting volume coil for magnetic resonance microscopy of the mouse brain. Journal of Magnetic Resonance, 2008, 191, 231-238.	2.1	24
146	Identifying Vulnerable Brain Networks in Mouse Models of Genetic Risk Factors for Late Onset Alzheimer's Disease. Frontiers in Neuroinformatics, 2019, 13, 72.	2.5	24
147	A symmetrical Waxholm canonical mouse brain for NeuroMaps. Journal of Neuroscience Methods, 2011, 195, 170-175.	2.5	23
148	A comparison of radial keyhole strategies for high spatial and temporal resolution 4D contrast-enhanced MRI in small animal tumor models. Medical Physics, 2013, 40, 022304.	3.0	23
149	Characterization of Subtle Brain Abnormalities in a Mouse Model of Hedgehog Pathway Antagonist-Induced Cleft Lip and Palate. PLoS ONE, 2014, 9, e102603.	2.5	23
150	Cardiac Micro–Computed Tomography for Morphological and Functional Phenotyping of Muscle LIM Protein Null Mice. Molecular Imaging, 2007, 6, 7290.2007.00022.	1.4	23
151	Studies on bromobenzene-induced hepatotoxicity usingin vivo MR microscopy with surgically implanted RF coils. Magnetic Resonance in Medicine, 1994, 31, 619-627.	3.0	22
152	Contribution of Magnetic Resonance Microscopy in the 12-Week Neurotoxicity Evaluation of Carbonyl Sulfide in Fischer 344 Rats. Toxicologic Pathology, 2004, 32, 501-510.	1.8	22
153	Tomographic digital subtraction angiography for lung perfusion estimation in rodents. Medical Physics, 2007, 34, 1546-1555.	3.0	22
154	Diffusion tensor magnetic resonance histology reveals microstructural changes in the developing rat brain. NeuroImage, 2013, 79, 329-339.	4.2	22
155	Semi-automated 3D segmentation of major tracts in the rat brain: comparing DTI with standard histological methods. Brain Structure and Function, 2014, 219, 539-550.	2.3	22
156	Quantitative mapping of trimethyltin injury in the rat brain using magnetic resonance histology. NeuroToxicology, 2014, 42, 12-23.	3.0	22
157	Whole mouse brain connectomics. Journal of Comparative Neurology, 2019, 527, 2146-2157.	1.6	22
158	Virtual Neuropathology: Three-Dimensional Visualization of Lesions Due to Toxic Insult. Toxicologic Pathology, 2000, 28, 100-104.	1.8	21
159	Quantitative blood flow measurements in the small animal cardiopulmonary system using digital subtraction angiography. Medical Physics, 2009, 36, 5347-5358.	3.0	21
160	Diffusion tractography of the rat knee at microscopic resolution. Magnetic Resonance in Medicine, 2019, 81, 3775-3786.	3.0	21
161	Hyperpolarized3He NMR Lineshape Measurements in the Live Guinea Pig Lung. Magnetic Resonance in Medicine, 1998, 40, 61-65.	3.0	20
162	A micro-CT analysis of murine lung recruitment in bleomycin-induced lung injury. Journal of Applied Physiology, 2008, 105, 669-677.	2.5	20

#	Article	IF	CITATIONS
163	Dynamic contrast-enhanced quantitative susceptibility mapping with ultrashort echo time MRI for evaluating renal function. American Journal of Physiology - Renal Physiology, 2016, 310, F174-F182.	2.7	20
164	GLIS1 regulates trabecular meshwork function and intraocular pressure and is associated with glaucoma in humans. Nature Communications, 2021, 12, 4877.	12.8	20
165	Active Staining of Mouse Embryos for Magnetic Resonance Microscopy. Methods in Molecular Biology, 2010, 611, 141-149.	0.9	20
166	A fast spin echo technique with circular sampling. Magnetic Resonance in Medicine, 1998, 39, 23-27.	3.0	19
167	Optimized radiographic spectra for small animal digital subtraction angiography. Medical Physics, 2006, 33, 4249-4257.	3.0	19
168	Ultrasonic disruption of the blood–brain barrier enables in vivo functional mapping of the mouse barrel field cortex with manganese-enhanced MRI. NeuroImage, 2010, 50, 1464-1471.	4.2	19
169	Temporal and spectral imaging with micro T. Medical Physics, 2012, 39, 4943-4958.	3.0	19
170	Altered diffusion tensor imaging measurements in aged transgenic Huntington disease rats. Brain Structure and Function, 2013, 218, 767-778.	2.3	19
171	An ontology-based segmentation scheme for tracking postnatal changes in the developing rodent brain with MRI. NeuroImage, 2013, 67, 375-384.	4.2	19
172	Hyperpolarized3He microspheres as a novel vascular signal source for MRI. Magnetic Resonance in Medicine, 2000, 43, 440-445.	3.0	18
173	A high-resolution interactive atlas of the human brainstem using magnetic resonance imaging. NeuroImage, 2021, 237, 118135.	4.2	18
174	Rapid production of specialized animal handling devices using computerâ€aided design and solid freeform fabrication. Journal of Magnetic Resonance Imaging, 2009, 30, 466-471.	3.4	17
175	Genetic dissection of the mouse CNS using magnetic resonance microscopy. Current Opinion in Neurology, 2009, 22, 379-386.	3.6	17
176	Continuing Education Course #3. Toxicologic Pathology, 2011, 39, 289-293.	1.8	17
177	Addendum to "Waxholm Space atlas of the Sprague Dawley rat brain―[NeuroImage 97 (2014) 374-386]. NeuroImage, 2015, 105, 561-562.	4.2	17
178	Dynamic contrast-enhanced MRI promotes early detection of toxin-induced acute kidney injury. American Journal of Physiology - Renal Physiology, 2019, 316, F351-F359.	2.7	17
179	MR microscopy at 7.0 T: Effects of brain iron. Journal of Magnetic Resonance Imaging, 1991, 1, 301-305.	3.4	16
180	Surface coil imaging of rat spine at 7.0 T. Magnetic Resonance Imaging, 1992, 10, 929-934.	1.8	16

#	Article	IF	CITATIONS
181	Application of MOSFET Detectors for Dosimetry in Small Animal Radiography Using Short Exposure Times. Radiation Research, 2008, 170, 260-263.	1.5	16
182	Cardiovascular phenotyping of the mouse heart using a 4D radial acquisition and liposomal Gd-DTPA-BMA. Magnetic Resonance in Medicine, 2010, 63, 979-987.	3.0	16
183	Micro-CT imaging assessment of dobutamine-induced cardiac stress in rats. Journal of Pharmacological and Toxicological Methods, 2011, 63, 24-29.	0.7	16
184	Denoising of 4D cardiac micro-CT data using median-centric bilateral filtration. , 2012, 8314, .		16
185	The Utility of Micro-CT and MRI in the Assessment of Longitudinal Growth of Liver Metastases in a Preclinical Model of Colon Carcinoma. Academic Radiology, 2013, 20, 430-439.	2.5	16
186	An analysis of the uncertainty and bias in DCEâ€MRI measurements using the spoiled gradientâ€recalled echo pulse sequence. Medical Physics, 2014, 41, 032301.	3.0	16
187	Accelerating quantitative susceptibility imaging acquisition using compressed sensing. Physics in Medicine and Biology, 2018, 63, 245002.	3.0	16
188	In vivo magnetic resonance imaging of the blue crab,Callinectes sapidus: Effect of cadmium accumulation in tissues on proton relaxation properties. The Journal of Experimental Zoology, 1992, 263, 32-40.	1.4	15
189	Quantitative analysis of hyperpolarized 3 He ventilation changes in mice challenged with methacholine. Magnetic Resonance in Medicine, 2010, 63, 658-666.	3.0	15
190	Reduction of artifacts in <i>T</i> ₂ â€weighted PROPELLER in highâ€field preclinical imaging. Magnetic Resonance in Medicine, 2011, 65, 538-543.	3.0	15
191	Comparison of 4D-MicroSPECT and MicroCT for Murine Cardiac Function. Molecular Imaging and Biology, 2014, 16, 235-245.	2.6	15
192	Distinguishing Plant Tissues with Magnetic Resonance Microscopy. American Journal of Botany, 1991, 78, 1704.	1.7	15
193	In vivo Magnetic Resonance Imaging of Blechnum Ferns: Changes in T1 and N (H) During Dehydration and Rehydration. American Journal of Botany, 1991, 78, 80.	1.7	15
194	Magnetic Resonance Imaging (MRI): A New Tool in Experimental Toxicologic Pathology. Toxicologic Pathology, 1988, 16, 386-389.	1.8	14
195	Progression of a focal ischemic lesion in rat brain during treatment with a novel glycine/nmda antagonist: An in vivo three-dimensional diffusion-weighted MR microscopy study. Journal of Magnetic Resonance Imaging, 1997, 7, 739-744.	3.4	14
196	Registration-based segmentation of murine 4D cardiac micro-CT data using symmetric normalization. Physics in Medicine and Biology, 2012, 57, 6125-6145.	3.0	14
197	Optimizing Diffusion Imaging Protocols for Structural Connectomics in Mouse Models of Neurological Conditions. Frontiers in Physics, 2020, 8, .	2.1	14
198	Cardiac micro-computed tomography for morphological and functional phenotyping of muscle LIM protein null mice. Molecular Imaging, 2007, 6, 261-8.	1.4	14

#	Article	IF	CITATIONS
199	Transition metal-chelate complexes as relaxation modifiers in nuclear magnetic resonance. Medical Physics, 1984, 11, 67-72.	3.0	13
200	MR "Microscopy―of the Rat Thorax. Journal of Computer Assisted Tomography, 1986, 10, 948-952.	0.9	13
201	Image optimization in a computed-radiography/photostimulable-phosphor system. Journal of Digital Imaging, 1989, 2, 212-219.	2.9	13
202	T1? imaging using magnetization-prepared projection encoding (MaPPE). Magnetic Resonance in Medicine, 2000, 43, 421-428.	3.0	13
203	Quantitative Neuromorphometry Using Magnetic Resonance Histology. Toxicologic Pathology, 2011, 39, 85-91.	1.8	13
204	3D Exploration of the Brainstem in 50-Micron Resolution MRI. Frontiers in Neuroanatomy, 2020, 14, 40.	1.7	13
205	Characterization complex collagen fiber architecture in knee joint using highâ€resolution diffusion imaging. Magnetic Resonance in Medicine, 2020, 84, 908-919.	3.0	13
206	An Experimental "Trans-Molybdenum―Tube for Mammography. Radiology, 1978, 127, 511-516.	7.3	12
207	Digital Synthesis of Lung Nodules. Investigative Radiology, 1985, 20, 933-937.	6.2	11
208	Magnetic Resonance Microscopy of Chemically-Induced Liver Foci. Toxicologic Pathology, 1989, 17, 613-616.	1.8	11
209	Magnetic Resonance Microscopy of the Rat Carotid Artery at 300 Megahertz. Investigative Radiology, 1994, 29, 822-826.	6.2	11
210	Development of a noncontact 3-D fluorescence tomography system for small animal in vivo imaging. Proceedings of SPIE, 2009, 7191, nihpa106691.	0.8	11
211	Multishot PROPELLER for highâ€field preclinical MRI. Magnetic Resonance in Medicine, 2010, 64, 47-53.	3.0	11
212	Multispectral imaging with three-dimensional rosette trajectories. Magnetic Resonance in Medicine, 2008, 59, 581-589.	3.0	10
213	Resolution and b value dependent structural connectome in ex vivo mouse brain. NeuroImage, 2022, 255, 119199.	4.2	10
214	Implementation Of Adaptive Filtration For Digital Chest Imaging. Optical Engineering, 1987, 26, 267669.	1.0	9
215	Functional imaging of the lung. Nature Medicine, 1996, 2, 1192-1192.	30.7	9
216	Magnetic resonance microscopy and histopathology: Comparative approach of bromobenzene-induced hepatotoxicity in the rat. Hepatology, 1998, 27, 526-532.	7.3	9

#	Article	IF	CITATIONS
217	High-resolution reconstruction of fluorescent inclusions in mouse thorax using anatomically guided sampling and parallel Monte Carlo computing. Biomedical Optics Express, 2011, 2, 2449.	2.9	9
218	Investigations on x-ray luminescence CT for small animal imaging. , 2012, 8313, 83130T.		8
219	4D MRI of polycystic kidneys from rapamycinâ€treated Clis3â€deficient mice. NMR in Biomedicine, 2015, 28, 546-554.	2.8	8
220	IN VIVO MAGNETIC RESONANCE IMAGING OF BLECHNUM FERNS: CHANGES IN T1 AND N(H) DURING DEHYDRATION AND REHYDRATION. American Journal of Botany, 1991, 78, 80-88.	1.7	7
221	A Newin VivoMethod for Quantitative Analysis of Stroke Lesions Using Diffusion-Weighted Magnetic Resonance Microscopy. NeuroImage, 1996, 3, 158-166.	4.2	7
222	Morphology of the Small-Animal Lung Using Magnetic Resonance Microscopy. Proceedings of the American Thoracic Society, 2005, 2, 481-483.	3.5	7
223	The INCF Digital Atlasing Program: Report on Digital Atlasing Standards in the Rodent Brain. Nature Precedings, 2009, , .	0.1	7
224	A comparison of sampling strategies for dual energy micro-CT. , 2012, , .		7
225	Localization of Metal Electrodes in the Intact Rat Brain Using Registration of 3D Microcomputed Tomography Images to a Magnetic Resonance Histology Atlas. ENeuro, 2015, 2, ENEURO.0017-15.2015.	1.9	7
226	Structural mapping with fiber tractography of the human cuneate fasciculus at microscopic resolution in cervical region. NeuroImage, 2019, 196, 200-206.	4.2	7
227	TBR-760, a Dopamine-Somatostatin Compound, Arrests Growth of Aggressive Nonfunctioning Pituitary Adenomas in Mice. Endocrinology, 2020, 161, .	2.8	7
228	Time course and mechanism of alterations in proton relaxation during liver regeneration in the rat. Hepatology, 1985, 5, 538-543.	7.3	6
229	Detection of bromobenzene-induced hepatocellular necrosis using magnetic resonance microscopy. Magnetic Resonance in Medicine, 1995, 34, 853-857.	3.0	6
230	Ventilation/perfusion imaging in a rat model of airway obstruction. Magnetic Resonance in Medicine, 2010, 63, 728-735.	3.0	6
231	Continuing Education Course #1. Toxicologic Pathology, 2011, 39, 267-272.	1.8	6
232	Maximization of contrast-to-noise ratio to distinguish diffusion and microcirculatory flow. Journal of Magnetic Resonance Imaging, 1991, 1, 39-46.	3.4	5
233	Modern Trends in Imaging VII: Magnetic Resonance Microscopy. Analytical Cellular Pathology, 2012, 35, 205-227.	1.4	5
234	Magnetic Resonance Imaging of Graded Skeletal Muscle Injury in Live Rats. Environmental Health Insights, 2014, 8s1, EHI.S15255.	1.7	5

#	Article	IF	CITATIONS
235	Four-dimensional MRI of renal function in the developing mouse. NMR in Biomedicine, 2014, 27, 1094-1102.	2.8	5
236	Ex Vivo MR Histology and Cytometric Feature Mapping Connect Three-dimensional in Vivo MR Images to Two-dimensional Histopathologic Images of Murine Sarcomas. Radiology Imaging Cancer, 2021, 3, e200103.	1.6	5
237	Simulation of mammographic x-ray spectra. Medical Physics, 1980, 7, 189-195.	3.0	4
238	Static and dynamic cardiac modelling: Initial strides and results towards a quantitatively accurate mechanical heart model. , 2010, , .		4
239	Functional Neuroimaging Using Ultrasonic Blood-brain Barrier Disruption and Manganese-enhanced MRI. Journal of Visualized Experiments, 2012, , e4055.	0.3	4
240	Morphological studies of the murine heart based on probabilistic and statistical atlases. Computerized Medical Imaging and Graphics, 2012, 36, 119-129.	5.8	4
241	Qualitative and Quantitative Neuropathology Approaches Using Magnetic Resonance Microscopy (Diffusion Tensor Imaging) and Stereology in a Hexachlorophene Model of Myelinopathy in Sprague-Dawley Rats. Toxicologic Pathology, 2020, 48, 965-980.	1.8	4
242	Microcephaly with altered cortical layering in GIT1 deficiency revealed by quantitative neuroimaging. Magnetic Resonance Imaging, 2021, 76, 26-38.	1.8	4
243	A multicontrast MR atlas of the Wistar rat brain. NeuroImage, 2021, 242, 118470.	4.2	4
244	Tractography of Porcine Meniscus Microstructure Using High-Resolution Diffusion Magnetic Resonance Imaging. Frontiers in Endocrinology, 2022, 13, .	3.5	4
245	Measurement and modeling of 4D live mouse heart volumes from CT time series. , 2007, , .		3
246	In vivo imaging of rat coronary arteries using bi-plane digital subtraction angiography. Journal of Pharmacological and Toxicological Methods, 2011, 64, 151-157.	0.7	3
247	Dynamic contrastâ€enhanced MR microscopy identifies regions of therapeutic response in a preclinical model of colorectal adenocarcinoma. Medical Physics, 2015, 42, 2482-2488.	3.0	3
248	Diffusion tensor imaging using multiple coils for mouse brain connectomics. NMR in Biomedicine, 2018, 31, e3921.	2.8	3
249	Mapping the peripheral nervous system in the whole mouse via compressed sensing tractography. Journal of Neural Engineering, 2021, 18, 044002.	3.5	3
250	Phenylephrine-modulated cardiopulmonary blood flow measured with use of X-ray digital subtraction angiography. Journal of Pharmacological and Toxicological Methods, 2011, 64, 180-186.	0.7	2
251	Free-space fluorescence tomography with adaptive sampling based on anatomical information from microCT. Proceedings of SPIE, 2010, 7757, .	0.8	1
252	A LabVIEW Platform for Preclinical Imaging Using Digital Subtraction Angiography and Micro-CT. Journal of Medical Engineering, 2013, 2013, 1-13.	1.1	1

#	Article	IF	CITATIONS
253	A timeâ€course study of actively stained mouse brains: Diffusion tensor imaging parameters and connectomic stability over 1 year. NMR in Biomedicine, 2022, 35, e4611.	2.8	1
254	Structural Connectivity of Human Inferior Colliculus Subdivisions Using in vivo and post mortem Diffusion MRI Tractography. Frontiers in Neuroscience, 2022, 16, 751595.	2.8	1
255	MR imaging of microcirculation in rat brain: Correlation with carbon dioxide-induced changes in blood flow. Journal of Magnetic Resonance Imaging, 1991, 1, 673-681.	3.4	0
256	Magnetic Resonance Microscopy of Toxic Renal Injury Induced by Bromoethylamine in Rats. Toxicological Sciences, 1991, 16, 787-797.	3.1	0
257	Helical dual source cone-beam micro-CT. , 2014, , .		0
258	Magnetic resonance histology. Journal of Magnetic Resonance Imaging, 2015, 42, 1-2.	3.4	0
259	Image-processing pipelines: applications in magnetic resonance histology. Proceedings of SPIE, 2016, , .	0.8	0
260	Magnetic Resonance Microscopy. The Electrical Engineering Handbook, 2006, , 15-1-15-14.	0.2	0
261	Magnetic Resonance Microscopy. The Electrical Engineering Handbook, 1999, , .	0.2	0